Redox Biology 68 (2023) 102939

Contents lists available at ScienceDirect

Redox Biology

journal homepage: www.elsevier.com/locate/redox

HDAC3 aberration-incurred GPX4 suppression drives renal ferroptosis and AKI-CKD progression

Lijun Zhang [a,b], Fang Chen [a], Jian Dong [b], Rong Wang [c], Guangyu Bi [c], Daoliang Xu [c], Yingwei Zhang [d], Yijun Deng [a], Wenjun Lin [e,**], Zhongzhou Yang [b,***], Wangsen Cao [a,b,c,*,1]

[a] Yancheng Medical Research Center of Nanjing University Medical School, Department of Central Laboratory, Yancheng First Hospital, Affiliated Hospital of Nanjing University Medical School, The First People's Hospital of Yancheng, Yancheng, China
[b] Nanjing University Medical School, Jiangsu Key Lab of Molecular Medicine, Nanjing, China
[c] Yangzhou Precision Research Institute of Kidney Disease, Department of Nephrology, Northern Jiangsu People's Hospital, Yangzhou, China
[d] Department of Respirology, Affiliated Drum Tower Hospital of Nanjing University Medical School, Nanjing, China
[e] Department of Nephrology, Shanghai Sixth People's Hospital Affiliated to Shanghai Jiao Tong University School of Medicine, Shanghai, China

ARTICLE INFO

Keywords:
AKI-CKD progression
HDAC3
GPX4
Ferroptosis
KLF5

ABSTRACT

Acute kidney injury (AKI) progression to chronic kidney disease (CKD) represents a unique renal disease setting characterized by early renal cellular injury and regulated cell death, and later renal fibrosis, of which the critical role and nature of ferroptosis are only partially understood. Here, we report that renal tubular epithelial ferroptosis caused by HDAC3 (histone deacetylase 3) aberration and the resultant GPX4 suppression drives AKI-CKD progression. In mouse models of AKI-CKD transition induced by nephrotoxic aristolochic acid (AA) and folic acid (FA), renal tubular epithelial ferroptosis occurred early that coincided with preferential HDAC3 elevation and marked suppression of a core anti-ferroptosis enzyme GPX4 (glutathione peroxidase 4). Intriguingly, genetic *Hdac3* knockout or administration of a HDAC3-selective inhibitor RGFP966 effectively mitigated the GPX4 suppression, ferroptosis and the fibrosis-associated renal functional loss. In cultured tubular epithelial cells, HDAC3 over-expression or inhibition inversely affected GPX4 abundances. Further analysis revealed that *Gpx4* promoter contains a typical binding motif of transcription factor KLF5 (Kruppel-like factor 5). HDAC3 and KLF5 inducibly associated and bound to *Gpx4* promoter upon AA treatment, leading to local histone hypoacetylation and GPX4 transactivation inhibition, which was blocked by RGFP966 and a KLF5 inhibitor ML264, respectively, suggesting that KLF5 co-regulated the HDAC3-incurred Gpx4 transcription inhibition. More importantly, in AKI-CKD mice receiving a GPX4 inactivator RSL3, the anti-ferroptosis and renoprotective effects of RGFP966 were largely abrogated, indicating that GPX4 is an essential downstream mediator of the HDAC3 aberration and renal ferroptosis during AKI-CKD transition. Together, our study identified a critical epigenetic pathway of ferroptosis during AKI-CKD transition and suggested that the strategies preserving GPX4 by HDAC3 inhibition are potentially effective to reduce renal ferroptosis and slow AKI-CKD progression.

1. Introduction

Acute kidney injury (AKI) and chronic kidney disease (CKD) clinically fall in two disease categories with different etiologies and pathogeneses, however more than 20 % of AKI cases even clinically recovered from initial AKI still progresses to CKD [1], of which the precise mechanisms are not well understood. AKI to CKD transition is mediated by multiple pathological events, including early tubular epithelial injury, endothelial dysfunction, inflammation, oxidative stress and later renal fibrosis, resulting in deteriorated renal functions or even end stage renal failure [2]. Renal tubular epithelia are the most abundant kidney residential cells and the vulnerable targets of AKI attacks, such as

* Corresponding author. Yancheng Medical Research Center of Nanjing University Medical School, Department of Central Laboratory, Yancheng First Hospital, Affiliated Hospital of Nanjing University Medical School, The First People's Hospital of Yancheng, Yancheng, China.
** Corresponding author.
*** Corresponding author.
E-mail addresses: linwenjun5@126.com (W. Lin), zhongzhouyang@nju.edu.cn (Z. Yang), wangsencao@nju.edu.cn (W. Cao).
[1] Leader contact.

https://doi.org/10.1016/j.redox.2023.102939
Received 26 September 2023; Accepted 17 October 2023
Available online 20 October 2023

ischemia reperfusion, nephrotoxicity, sepsis, or urinary tract obstruction. The injured renal epithelia lose their phenotypes, exhibit senescence, secrete proinflammatory and profibrotic cytokines and undergo various forms of regulated cell death, such as necrosis, apoptosis, necroptosis, ferroptosis and pyroptosis [3]. Although the injured epithelia possess intrinsic repair capacities and some forms of regulated cell death are reversible [4,5], such that the survival cells can reenter mitosis, regenerate tubular epithelium and restore kidney architecture, it is believed that impaired repairing process and severe tubular cell death perpetuate AKI pathogenesis and contribute to AKI-CKD progression [6].

Ferroptosis is a distinct form of regulated cell death characterized by iron-dependent accumulation of lipid peroxides and mitochondrial membrane damage [7]. Many factors such as impaired metabolisms of amino acids and lipids, iron handling, mitochondrial activity or redox response contribute to ferroptosis, in which the dysregulation of glutathione GSH/GPX4 (glutathione peroxidase 4) signaling plays a key role [8,9]. GSH generated from glutamic acid, cysteine and glycine is a scavenger of free radicles and a cofactor of GPX4 [10]. Insufficient GSH generation reduces the synthesis of GPX4, which is capable of detoxifying lipid hydroperoxides (L-OOH) to lipid alcohols (L-OH), thus blocking ferroptosis [11]. Ferroptosis is causally involved in various pathophysiologies, such as cancers, ischemic reperfusion injuries, neurodegenerative disorders, cardiovascular and kidney diseases [12], In particular, *Gpx4* knockout mice develop spontaneous renal ferroptotic alterations and acute renal failure [13], and several small chemical compounds preserving GPX4 beneficially regulate renal ferroptosis [13–16]. GPX4 inactivation or depletion is a characteristic of ferroptosis [17], but its transcription regulation is less understood and likely involves aberrant epigenetic modifications [18]. Recent studies indicate that the transcription suppression of a number of anti-ferroptotic genes, including *Gpx4*, is regulated by histone deacetylase HDAC1, 2 and 3, which greatly affects neuronal ferroptosis [19,20], however the particular HDAC isoform(s) responsible for the *Gpx4* suppression and its functional relevance to kidney diseases are unknown.

HDAC1, 2 and 3 belong to class I HDACs (1, 2, 3, and 8). Other mammalian HDAC classes include class II (HDAC4, 5, 6, 7, 9 and 10), class III (Sirt1-7) and class IV (HDAC11) that display different structural characters, subcellular distribution or catalytic cofactor dependency [21]. Unlike histone acetyltransferases that add acetyl-groups to lysine residues of histones and facilitate gene transcription, HDACs remove acetyl group and induce gene transcription inhibition [22]. It is now generally accepted that aberrant epigenetic protein/histone acetylation modifications causally affect AKI-CKD transition via different cellular processes and signaling pathways [23,24]. We have previously discovered that HDAC3 among other HDAC class I members is preferentially upregulated in fibrotic and CKD mouse kidneys induced by adenine and UUO (Unilateral ureter obstruction) [25,26]. HDAC3 functions exclusively as a key component of a transcriptional repression complex containing transcriptional repressors, such as NCoR and SMRT [27,28], and other transcription cofactors [29]. Thus, HDAC3 aberration might regulate *Gpx4* transcription and renal ferroptosis during AKI-CKD progression.

In this study, we investigated the critical role and nature of renal ferroptosis during AKI-CKD progression. We focused on GPX4 suppression and its potential epigenetic regulation by HDAC3. We performed the study with both genetic and pharmacological approaches in two mouse models of AKI-CKD transition incurred by nephrotoxic aristolochic acid (AA) and high dose of folic acid (FA) [30–33]. Our study will help to better understand the critical epigenetic regulatory events of ferroptosis during AKI-CKD transition and gain insights into the potential gene-targeted strategies to intervene the processes.

2. Materials and methods

2.1. Animal study

C57BL/6J male mice of around 8-weeks of age were from the Model Animal Research Center of Nanjing University. The generation and characterization of the conditional *Hdac*3 knockout mice (*Hdac3*$^{fl/fl/Cre-ERT2}$, *Hdac3*KO) have been previously reported [25]. Induction of *Hdac3* knockout was achieved by intraperitoneal injection of tamoxifen (HY-13757A/CS-2870, MCE, USA, 1 mg per mouse, dissolved in corn oil containing 10 % ethanol) for 5 consecutive days and maintained for 7 additional days to ensure *Hdac3* knockout. All experiments were performed according to the protocol approved by the Animal Care and Use Committee of the Institutional Animal Care Committee (IACUC) of Yangzhou University (yzu-lcyxy-n005), complied with the ARRIVE guidelines and the European Directive 2010/63/EU. Mice were free to diet and water and maintained at 25 ± 2 °C temperature and regular lighting conditions (12 h light/dark cycles).

Mouse models of AKI-to-CKD transition were established by intraperitoneal injection of aristolochic acid I (AA) [32,33] or folic acid (FA) [30,31]. We performed three sets of mouse experiments. For intervention experiments, C57BL/6J mice were assigned to four groups (n = 6 mice per group): (1) vehicle control; (2) RGFP966 (S7229, Selleck, USA, 10 mg/kg subcutaneous injection starting the first day and following every other day) [25], or liproxstatin-1 (Lip-1) (10 mg/kg, HY-12726, MCE, USA, daily intraperitoneal injection) [34]; (3) AKI-to-CKD model mice: Aristolochic acid I sodium salt (AA, A5512, Sigma-Aldrich, USA, 5 mg/kg/day intraperitoneal injection) or folic acid (FA, S4605, Selleck, USA, a single 250 mg/kg intraperitoneal injection, diluted in 0.3 mM sodium bicarbonate); and (4) RGFP966 or liproxstain-1intervention starting 24h after AA/FA delivery [32,33]. For experiments to determine the role of HDAC3 in AKI-CKD transition, both *Hdac*3KO (*Hdac3*$^{fl/fl/Cre-ERT2}$) and the control (*Hdac3*$^{fl/fl}$) mice were intraperitoneally injected with tamoxifen as described above to induce HDA3 knockout before AA or FA treatment. For experiments to determine the role of GPX4 in the RGFP966 intervention, C57BL/6J mice were pre-treated with or without RSL3 (5 mg/kg, daily intraperitoneal injection, HY-100218A/CS-5650, MCE, USA) [35,36], and then subjected to control, RGFP966, AA and RGFP966/AA intervention. The mice were sacrificed via intraperitoneal injection of sodium pentobarbitone (240 mg/kg) at days 3 or 14 after experiment completion. The mouse kidneys were surgically collected, embedded for histological assay or stored at −80 °C for further analysis.

2.2. Human kidney samples

Fourteen human kidney samples were obtained from CKD patients (43–65 years old) who received renal biopsy for clinical diagnosis purpose at Yancheng First People's Hospital, Jiangsu, China. The normal controls were paracancerous tissues from renal tumor patients underwent tumor-removal surgery. The study was approved by the hospital ethics committee (2022-K101) and written informed consent was received from all subjects.

2.3. Western blotting

Western blotting assays of renal tissues or cell lysates were performed essentially as before [25]. The protein samples were washed with PBS and then lysed with RIPA buffer (P0013B, Beyotime, China) with a protease inhibitor cocktail (4693116001, Roche, Switzerland) and PhosSTOP (4906837001, Roche, Switzerland) for 30 min. The protein concentration was quantified by a BCA Protein Assay Kit (P0012, Beyotime, China) and equal amounts of proteins were analyzed on One-Step PAGE Gel (8%–12 %, Vazyme, China) and then transferred onto PVDF membranes (Millipore, IPVH00010). The proteins were then blocked with 5 % bovine serum albumin (BSA, 4240GR500, BioFroxx,

Germany) in Tris-buffered saline-Tween 20 (TBST, 9997, CST, USA) and then incubated with primary antibodies. The anti-bodies used were as following: GPX4 (A11243, 1:2000,ABclonal, China); HDAC1 (1:1000, #5356P, Cell Signaling Technology, USA); HDAC2 (1:1000, #5113P, Cell Signaling Technology, USA); HDAC3 (1:2000, A16462, ABclonal, China); HDAC8 (1:1000, A5829, ABclonal, China); 4-Hydroxynonenal (ab46545, 1:500, Abcam, UK); KLF5 (AF04622, 1:1000, AiFang biological, China); E-cadherin (GB11082, 1:2000) and type 1 collagen (GB11022-2, 1:500) from Servicebio, China; α-SMA (sc-32251, 1:500, Santa Cruz, USA); histone 3 (4499T, 1:1000, Cell Signaling Technology, USA); acetylated histone 3 (Ac-H3, 06–599, 1:1000, Milli-pore, USA); GAPDH (60004-1-Ig, 1:5000, Proteintech, USA). After primary antibody incubation, the blots were washed and incubated with secondary antibodygoat anti-rabbit IgG-HRP (YFSA02, 1:10000) or goat anti-mouse IgG-HRP (YFSA01, 1:10000) from Yifeixue biotech, China. The detection was visualized with an ECL plus western blotting detection system (Vazyme, China). The molecular weight marker used was WJ102 (EpiZyme, China) or MP102 (Vazyme, China). The protein levels were analyzed by ImageJ software and data were presented as fold changes relative to the loading controls.

2.4. H&E, Masson trichrome and immunohistochemistry staining

Renal section preparations and staining by haematoxylin and eosin (H&E), Masson trichrome and immunohistochemistry (HDAC3 and GPX4) were performed essentially as before [25]. Renal tubule damage was assessed by H&E staining on a scale ranging from 0 to 4 based on tubular epithelial cell swelling, vacuolization, interstitial expansion, and inflammatory cell infiltration (0, no damage or <10 % injury; 1, 10–25 % injury; 2, 25–50 % injury; 3, 50–75 % injury; 4, >75 % injury) [37]. Renal fibrosis stained by Masson trichrome was assessed as the percentage of collagen deposition area over the total renal area. Ten randomly-selected visual fields in each section were scored and averaged. The intensity of immunohistochemical staining of renal patient samples was assessed based on a 0 to 3 (0, minimum staining; 1, weak staining; 2, moderate staining; 3, strong staining) scoring method [38] from six randomly-selected fields of each section using ImageJ software. Microphotographs were obtained with an Olympus DP74 light microscope and all assessments were performed in a double-blind manner.

2.5. TUNEL assay

TUNEL (terminal deoxynucleotidyl transferase mediated dUTP nick-end labeling) assays of kidney sections or HK2 cells were conducted with a Fluorescein (FITC) TUNEL Detection Kit (G1501, Servicebio, China) or a TUNEL BrightRed Kit (A113-03, Vazyme, China) according to the manufacturers' protocols. The kidney tissues were fixed with 4 % paraformaldehyde, embedded in paraffin, sectioned, dewaxed and rehydrated, and cells were prepared with cell slides and fixed 4 % paraformaldehyde, before TUNEL assays. The percentages of positively-stained cells over total cells from 10 randomly-selected fields were counted in a double-blinded manner. The images were captured with an Olympus FV3000 confocal fluorescent microscope.

2.6. Perl's Prussian blue staining

Perl's Prussian blue staining of renal sections detecting hemosiderin was performed with a commercial kit (G1029, Servicebio, China) with signal enhancement by DAB (3,3′-diaminobenzidine). Briefly, potassium ferrocyanide was used to separate trivalent iron/ions from proteins and produce water-insoluble blue ferrocyanide precipitation. Subsequently, DAB was added to the reaction that produced brown compounds. The brown color area over total area from 10 randomly-selected fields of each section were calculated and averaged in a double-blinded manner using Image J software.

2.7. Electron microscopy (EM) examination

Transmission electron microscopy examination was performed by a commercial biotech company (ShangDong Weiya Bio Co., LTD, China). Briefly, the freshly-dissected renal tissues were cut into small pieces (1 mm^3) and quickly immersed in aldehyde fixation solution at room temperature for 15 min, and then transferred to 4 °C for cryopreservation. The samples were then dehydrated, embedded and sectioned, and observed under TEM. Ten randomly-selected visual fields of each sample were examined and images captured.

2.8. HDAC3 activity assay

HDAC3 activities of renal tissues were analyzed with an HDAC Activity/Inhibition Direct Assay Kit (Colorimetric) (P-4034, Epigentek, USA) according to the manufactory's protocol. In brief, the acetylated substrates were incubated with the renal tissue homogenates in presence or absence HDAC3 inhibitor RGPF966, and then with a specific primary antibody that recognized the deacetylated substrates. After incubation with an enzyme-conjugated secondary antibody and the enzyme substrates, the samples were then measured at 450 nM with a multifunctional microplate reader. The HDAC activities were calculated as fold changes relative to the control and the reduced activities elicited by RGFP966 was considered the HDAC3 activity [39].

2.9. Cells and cell culture

Human kidney tubular HK2 cells and human embryonic kidney HEK293 cells (ATCC, USA) were cultured in DMEM/F12 (Biosharp, China) or DMEM medium (Wisent, China) with 10 % fetal bovine serum (FBS, 04-001-1ACS, Biological Industries, Israel) and 1 % penicillin/streptomycin (15140122, Gibco, USA) at 37 °C in a humidified 5 % CO_2 incubator. Cells were treated with AA, RGFP966, ML264 (KLF5 inhibitor, HY-19994/CS-5628, MCE, USA) and/or RSL3 as indicated.

Primary renal tubular epithelial cells were isolated from 8-week-old C57BL/6J, *Hdac*3KO (*Hdac3*$^{fl/fl/Cre-ERT2}$) or the control (*Hdac3*$^{fl/fl}$) mice following previously-established protocols [40,41], excepted that *Hdac*3KO and the control mice were first injected with tamoxifen to knockout *Hdac3* as described above. Briefly, the fresh renal cortex was dissected, minced and digested in 1 mg/ml collagenase for 40 min at 37 °C, and then the mashed tissues were centrifuge at 1000 rpm for 5 min at 4 °C. The tubular tissues were isolated by 31 % Percoll gradients. Finally, the tubular cells were resuspended in DMEM/F12 medium supplemented with 10 % fetal bovine serum, 1 % penicillin/streptomycin and hormonal mixture (5 μg/ml insulin, 1.25 ng/ml prostaglandin E1, 34 pg/ml triiodothyronine, 5 μg/ml transferrin, 1.73 ng/ml sodium selenite, 18 ng/ml hydrocortisone, and 25 ng/ml epidermal growth factor, all from Sigma-Aldrich, US). The cells were cultured for 4–7 days with medium changed every 24–48 h until reaching 60%–80 % confluences.

2.10. C11-BODIPY staining

C11-BODIPY (Boron dipyrromethane difluoride) is a fatty acid analog with specific fluorescent properties in a visible spectrum of red range (emission maximum 595 nm), but shifts to green once oxidized (emission maximum 510 nm) [42]. We performed the assay with C11-BODIPY agent (D3861, Thermo Fisher, USA) and followed the manufacturer's protocol. Briefly, HK2 cells seeded in a 6-well plate under various treatments were incubated with C11-BODIPY dye (10 μM dissolved in DMSO) for 1 h. Excess C11-BODIPY was removed by washing the cells twice with PBS. The cells were observed under an Olympus FV3000 confocal fluorescent microscope with excitation/emission wavelengths of 488/510 nm for oxidized- (O-) BODIPY or of 581/591 nm for Non-oxidized- (N-) BODIPY, respectively. The average intensity of the fluorescent signals adjusted by cell numbers from six

randomly-selected fields was calculated with ImageJ software.

2.11. Plasmid construction and cell transfection

The murine *Gpx4* promoter reporter plasmid was constructed in pGL3-luc plasmid by inserting a PCR-amplified mouse *Gpx4* promoter fragment (2000 bp) at XhoI and HindIII sites (forward primer: CCGCTCGAGCTCAGGAGGGTGAAGTAGGG and reverse primer: CCCAAGCTTCAGCCAATGG GAAGCCTG, the enzymatic sites were underlined), and the cloned sequences were confirmed by DNA sequencing. A plasmid overexpressing flag-tagged HDAC3 has been previously described [25,43]. The plasmid was transfected into HEK293 cells with Lipofectamine 3000 reagents (Invitrogen, USA) following the manufacturer's instruction.

2.12. Luciferase assay

HEK293 cells were transfected with reporter plasmids *Gpx4*p-luc, plus a renilla luciferase plasmid as internal control. After 12 h of transfection, AA, RGFP966, or ML264 was added to the transfected cells. Twenty-four hours later, luciferase activities were assessed from the harvested total cell lysates using a dual luciferase reporter assay kit (E1910, Promega, USA). The luciferase activities of the *Gpx4* promoter reporter were normalized to renilla's and reported as relative fold changes.

2.13. Reverse-transcription PCR (RT-PCR) or quantitative real-time PCR (qRT-PCR)

RT-PCR or qRT-PCR detection of GPX4 and HDAC3 mRNAs in renal tissue was performed essentially as before [25]. Briefly, total RNAs were extracted from renal tissues by Trizol method (15596026, Invitrogen, USA). Equal amounts of mRNA were reversely transcribed to cDNA using a HiScript RT SuperMix kit (R122-01; Vazyme, China). Quantitative real-time PCR (qRT-PCR) was performed with ChamQ Universal SYBR qPCR Master Mix (Q711-02; Vazyme, China) on a Viia 7 quantitative real-time PCR instrument (Thermo-Fisher Scientific, USA). PCR amplification profiles were (35 cycles at 95 °C for 30 s, at 58 °C for 30 s, and at 72 °C for 30 s), which were performed with following primers: *Gpx4*F: CCCATTCCTGAACCTTTCAA, *Gpx4*R: GCACACGAAACCCCTGTACT; *Hdac3*F: CCCCACCAATATGCAGGGTT, *Hdac3*R: CAGAAGCCAGAGGCCTCAAA; *Gapdh*F: TATGTCGTGGAGTCTACTGGTGT; *Gpadh*R: GTCATCATACTTGGCAGGTTTCT. RT-PCR products were separated on a 1.5 % agarose gel and visualized under UV light and the qRT-PCR quantitation was performed by $2^{-\Delta\Delta Ct}$ method and expressed as relative fold changes.

2.14. Co-immunoprecipitation (Co-IP)

Co-IP was performed reciprocally as before [25]. The kidney lysates were first immunoprecipitated with antibody to HDAC3 or KLF5, or isoform-matched immunoglobulin (IgG) (Beyotime, China) overnight, and then incubated with Protein A + G Magnetic Beads (Beyotime, China) and washed. The immunoprecipitates were eluted and subjected to western blot analysis with antibodies to KLF5 or HDAC3, respectively. The non-immunoprecipited lyates served as the internal controls.

2.15. Chromatin immunoprecipitation PCR (ChIP)

ChIP assay of renal tissues was performed essentially as before [25] with a ChIP assay kit (P2078-4, Beyotime, China) following the manufacturer's instructions. The immunoprecipitation assay was performed first with antibody to HDAC3, KLF5, NCoR (sc-8994, Santa Cruz, USA) or acetylated histone 3 (Ac-H3, 06–599, Milli-pore, USA) at 4 °C overnight. The starting (input) and immunoprecipitated DNAs were further amplified by RT-PCR and qRT-PCR, respectively, with primer set *Gpx4*F: GGGGATGACTTTGACACGC and *Gpx4*R: GCCTGAATGAAGGGACGG, which covers *Gpx4* proximal promoter locus (−239 to −14, relative to the transcription starting site), which contains a putative KLF5 binding motif (−43/gccccgccca). The RT-PCR products were analyzed by 1.5 % agarose gels and visualized under UV light and the qRT-PCR quantification was performed by $2^{-\Delta\Delta Ct}$ method and expressed as relative fold changes.

2.16. Serum creatinine (Cre) and blood urea nitrogen (BUN) assay

Serum creatinine (Cre) and blood urea nitrogen (BUN) were measured essentially as before [44]. In brief, the experimental mice were anesthetized and mouse blood was collected from the orbital sinus with a capillary glass tube, centrifuged at 4000 rpm for 20 min at 4 °C, and the serum was taken. The assays were performed with a Creatinine Assay kit (D799853, Sangon Biotech, China) and a Urea Nitrogen Assay kit (D799850, Sangon Biotech, China), respectively, following manufacturer's assay protocols.

2.17. Malondialdehyde (MDA) assay

Renal tissue malondialdehyde (MDA) were measured with a Lipid Peroxidation MDA Assay Kit (S0131S, Beyotime, China) according to the manufacturer's instruction. The tissue homogenates were mixed with MDA working solution and boiled at 100 °C for 15 min, and then the absorbance at 532 nM was measured with a multifunctional microplate reader (Molecular Devices M3, USA). Data were expressed as the fold changes related to the control.

2.18. Statistical analysis

Data analyses were performed with GraphPad Prism. The data normal distributions and the assumptions of homogeneity of variance were assessed by Shapiro-Wilk test and Levene's test, respectively. Statistical differences analysis were assessed by Student's *t*-test, two-way analysis of variance (ANOVA), or ANOVA followed by Tukey's post hoc tests for comparisons of multiple group comparisons. Data were presented as means ± SEM of animal study, means ± SD for repeated cell assays, or Box-and-whisker plots in which midline represents median, box is the 25th-75th percentiles and whiskers are minimum and maximum. $P < 0.05$ was defined as statistically significant.

3. Results

3.1. Mouse AKI-CKD kidneys display aberrant HDAC3 elevation, GPX4 suppression and tubular epithelial ferroptosis

As an initial step to explore the possible role of epigenetic renal ferroptosis in AKI-CKD transition, we adapted two well-known AKI-CKD mouse models induced by repeated peritoneal injections of low dose nephrotoxic aristolochic acid (AA) and a single high dose injection of folic acid (FA), the latter forms crystal and deposits in lumen, leading to obstructive nephropathy [45,46]. We examined the renal sections at day 3 and day 14 representing AKI and fibrotic CKD stage, respectively [47]. As anticipated, mice receiving AA or FA for 3 days started to display extensive tubular epithelial injury (score 0 of control vs. 1.05 ± 0.07 of AA3d and 2.07 ± 0.08 of AA14d, $^*P < 0.05$; 1.1 ± 0.07 of FA3d and 2.1 ± 0.07 of FA14d, $^*P < 0.05$). Masson trichrome-stained fibrotic collagen deposition was milder at day 3 but more severe at day 14 (3.29 ± 0.23 % of control vs. 4.83 ± 0.79 % of AA3d and 13.40 ± 0.89 % of AA14d, $^*P < 0.05$; 4.67 ± 1.51 % FA3d and 12.72 ± 0.6 % of FA14d, $^*P < 0.05$). Meanwhile, Perl's Prussian blue staining revealed increased iron accumulation (1 ± 0.06 % of control vs.6.66 ± 0.48 % of AA3d and 4.92 ± 0.41 % of AA14d, $^*P < 0.05$; 6.98 ± 0.24 % of FA3d and 4.89 ± 0.34 % of FA14d, $^*P < 0.05$), and TUNEL assay, a sensitive way to stain apoptotic and ferroptotic cells [13], detected substantial positive cells at

day 3 and day 14 (2.09 ± 0.24 % of control vs.19.67 ± 0.97 % of AA3d and 15.84 ± 1.30 % of AA14d, *$P < 0.05$; 20.04 ± 0.96 % of FA3d and 16.1 ± 1.38 % of FA14d, *$P < 0.05$, Fig. 1a and b). Further examinations of renal tissues by western blotting revealed progressive and adverse expression of myofibroblast marker α-SMA, epithelial marker E-cadherin and extracellular matrix protein type 1 collagen after AA or FA treatment. Notably, HDAC3 was markedly upregulated with concomitant GPX4 downregulation and induction of lipid peroxidation marker 4-hydroxynonenal (4-HNE) (Fig. 1c and d). We further confirmed by electron microscopy examination that AA or FA treatment induced broad mitochondrial alterations of ferroptotic characters, such as smaller mitochondria and reduced or diminished mitochondrial crista (Fig. 1e). These results indicate that renal GPX4 suppression and ferroptosis occur early during AKI-CKD transition and closely correlate with aberrant HDAC3 elevation.

3.2. AA and FA induce inverse HDAC3 upregulation and GPX4 suppression in renal tubules

We further verified that HDAC3 among other HDAC I family members HDAC1, 2, and 8 was preferentially upregulated in AA and FA-treated kidneys (Fig. 2a and b), a pattern similar to that of UUO (unilateral ureteral obstruction) and adenine models [25,26]. Ferroptosis likely affects a broad spectrum of renal cell types. We found by immunohistochemical staining that GPX4 was enriched in tubular epithelial cells of the normal renal section, but drastically decreased after three days of AA or FA treatment (Fig. 2c, the right panel). In contrast, HDAC3 expression level was low, but markedly increased in a similar cell distribution (Fig. 2c, the left panel). To determine the stage of the expression alterations, we performed RT-PCR and found that AA or FA treatment significantly increased HDAC3 and decreased GPX4 mRNAs (Fig. 2d and e), suggesting that the inverse expression alterations of HDAC3 and GPX4 occurred substantially at transcriptional levels. We also stained 14 renal biopsy samples from CKD patients with severe

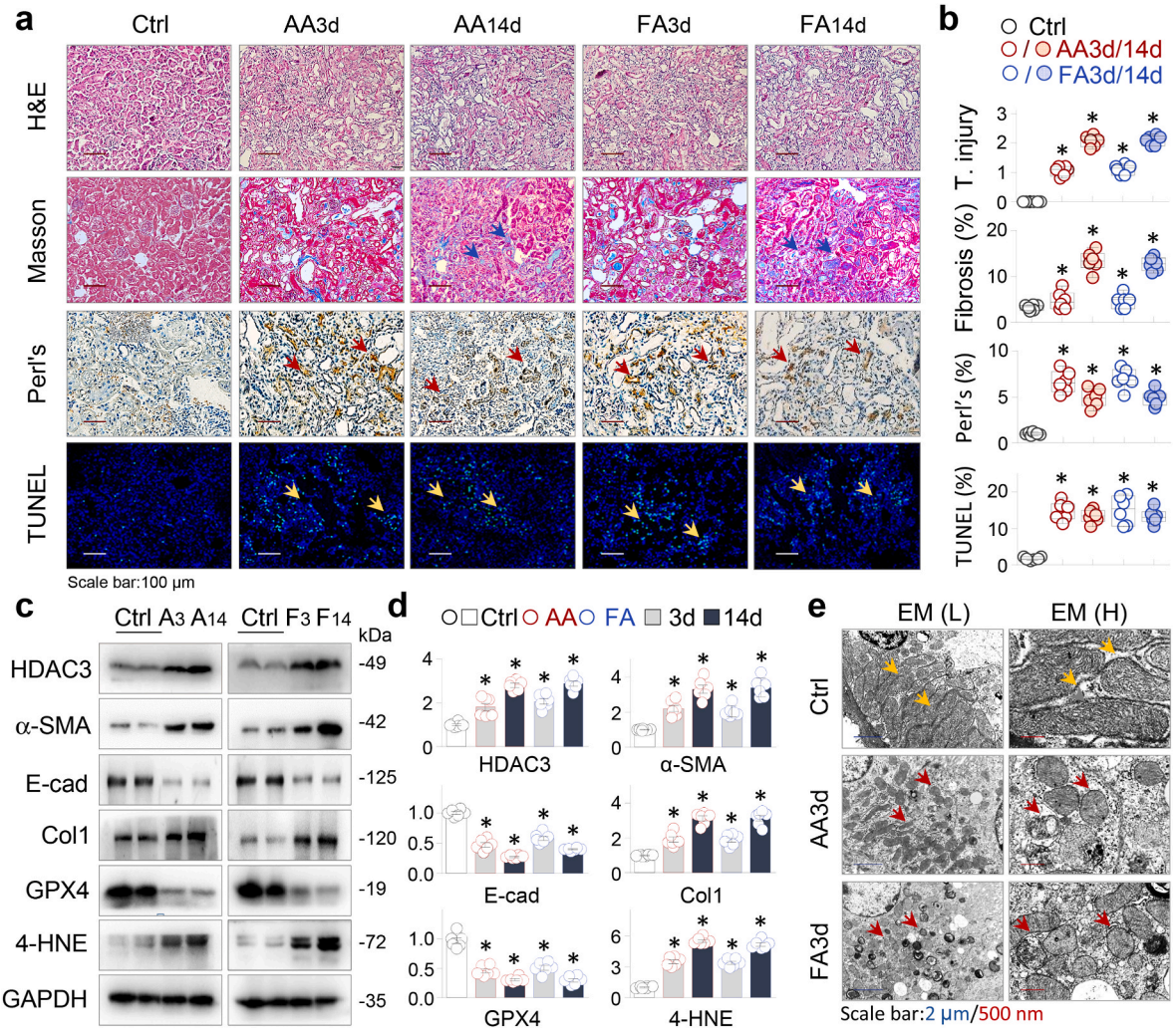

Fig. 1. AKI-CKD mice induced by AA (aristolochic acid) or FA (folic acid) display aberrant HDAC3 elevation, GPX4 suppression and ferroptosis. C57BL/6J mice were subjected to AA (5 mg/kg, daily intraperitoneal injection) or FA (250 mg/kg, single intraperitoneal injection) for 3 and 14 days (AA, A3/A14 and FA, F3/F14, six mice in each group). **(a)** Representative photomicrographs of kidney sections (Haematoxylin & eosin, Masson's trichrome staining, Perl's staining and TUNEL staining) from control and AA- or FA-treated mice. The collagen and iron depositions and TUNEL-positive cells were indicated by arrows. **(b)** Quantitation of 1a. Data were presented as Box-and-whisker plots with data points. *$P < 0.05$ vs. vehicle control (Ctrl), Student's *t*-test. **(c)** Western blotting. Renal tissue homogenates were assayed for HDAC3, α-SMA, E-cadherin (E-cad), Collagen I (Col1), GPX4 and 4-HNE. Two representative samples from each group were shown. GAPDH served as loading control. **(d)** Quantification of Fig. c. Data were presented as means ± SEM. *$P < 0.05$ vs. controls, Student's *t*-test. **(e)** Representative EM images of renal tissues from Ctrl, AA- or FA-treated mice (3 days) at low (L) and high (H) powers. Normal and ferroptotic mitochondria were indicated by yellow or red arrows, respectively. (For interpretation of the references to color in this figure legend, the reader is referred to the Web version of this article.)

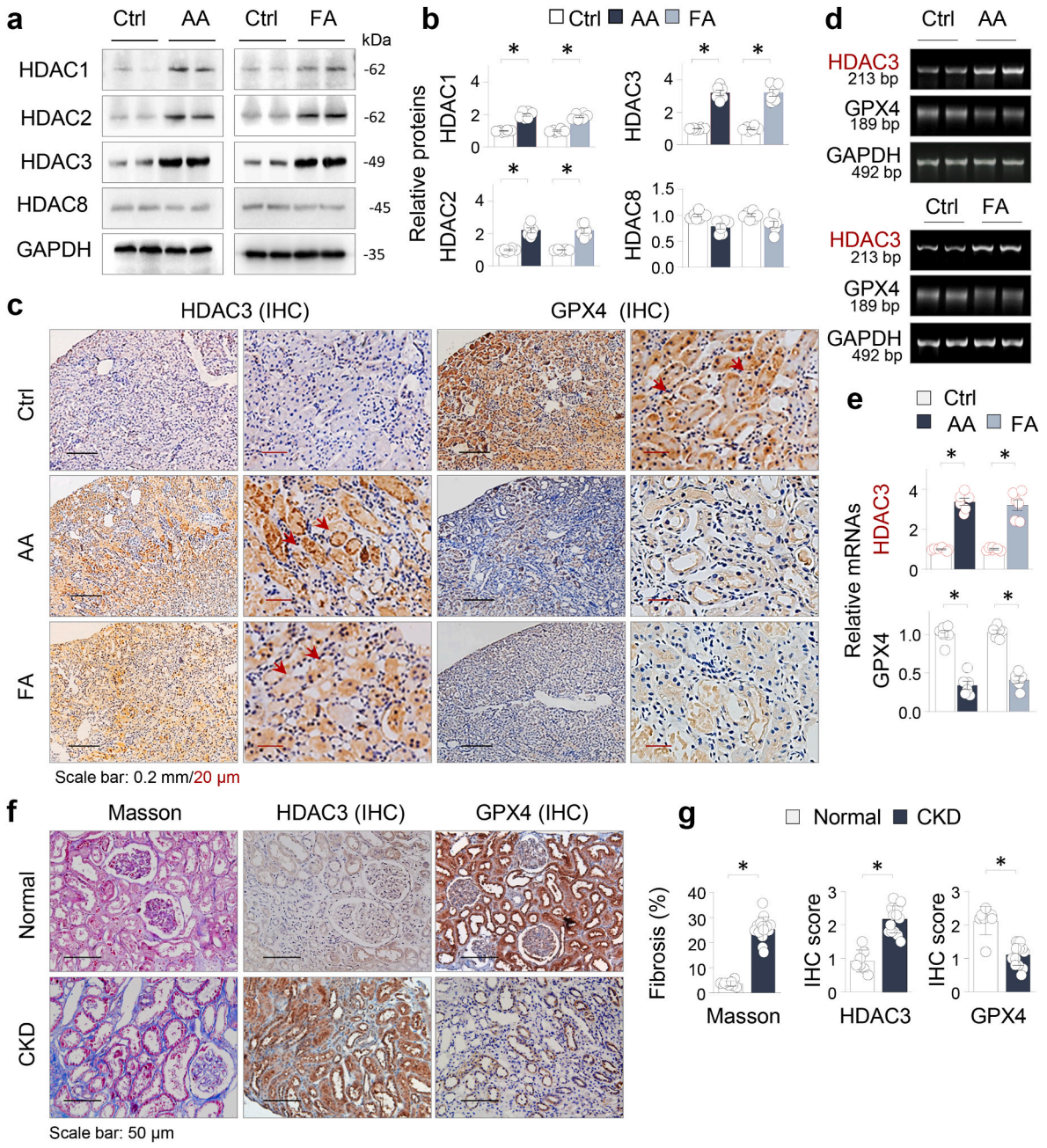

Fig. 2. AA (aristolochic acid) and FA (folic acid) induce inverse HDAC3 upregulation and GPX4 suppression in renal tubules. (a) Western blotting. Renal homogenates from control and the AA or FA-treated mice for 3 days were examined for HDAC1, HDAC2, HDAC3 and HDAC8. GAPDH served as loading control. Two representative samples from each group were shown. **(b).** Quantification of Fig. 2a. Data were presented as mean ± SEM, n = 6. *P < 0.05, Student's *t*-test. **(c)** Representative photomicrographs of kidney sections from control (Ctrl) and AA or FA-treated mice (3 days) stained for HDAC3 and GPX4 by immunohistochemistry (IHC) staining. Positively-stained tubular cells were indicated by arrows. **(d)** RT-PCR of renal tissues from the control (Ctrl) or AA-/FA-treated mice (n = 6) for HDAC3 and GPX4 mRNAs. *Gapdh* served as internal control. Two samples from each group were shown. **(e)** Quantification of Fig. 2d. Data were presented as means ± SEM. *P < 0.05, Student's *t*-test. **(f)** Representative photomicrographs of kidney sections from renal patients (Normal and CKD) stained by Masson trichrome for renal fibrosis and immunohistochemistry (IHC) for HDAC3 and GPX4. **(g)** Quantifications renal fibrosis and staining scoring of HDAC3 and GPX4 of the two groups (Normal, n = 7; CKD, n = 14). Data were presented as means ± SD. *P < 0.05, Student's *t*-test.

renal fibrosis (Fig. 2f and g) and found that comparing to 7 normal controls, the CKD renal sections showed increased HDAC3 but much reduced GPX4 staining (Fig. 2f and g), consistent with the mouse IHC staining patterns.

3.3. *HDAC3 knockout resists the GPX4 suppression, renal ferroptosis and fibrosis in AKI-CKD mice*

To gain insight into the potential role of the HDAC3 aberration in the ferroptosis and AKI-CKD transition, we generated a strain of conditional *Hdac3* knockout mice (*Hdac3*$^{-/-}$/CreER, *Hdac3*KO) that resist to UUO and adenine-induced kidney injuries [25,26]. We treated *Hdac3*KO mice with AA or FA and found that the mice developed much less fibrotic alterations (5.13 ± 0.40 % of *Hdac3*KO/AA mice vs. 12.53 ± 0.87 % of WT/AA; 4.85 ± 0.35 % of *Hdac3*KO/FA vs. 12.42 ± 0.56 % of WT/FA mice, *P < 0.05, Fig. 3a and b) and TUNEL-positive cells (7.34 ± 0.87 % of *Hdac3*KO/AA vs. 15.01 ± 0.46 % of WT/AA mice; 6.87 ± 0.75 % of *Hdac3*KO/FA vs. 14.87 ± 0.46 % of WT/FA mice, *P < 0.05, Fig. 3a and

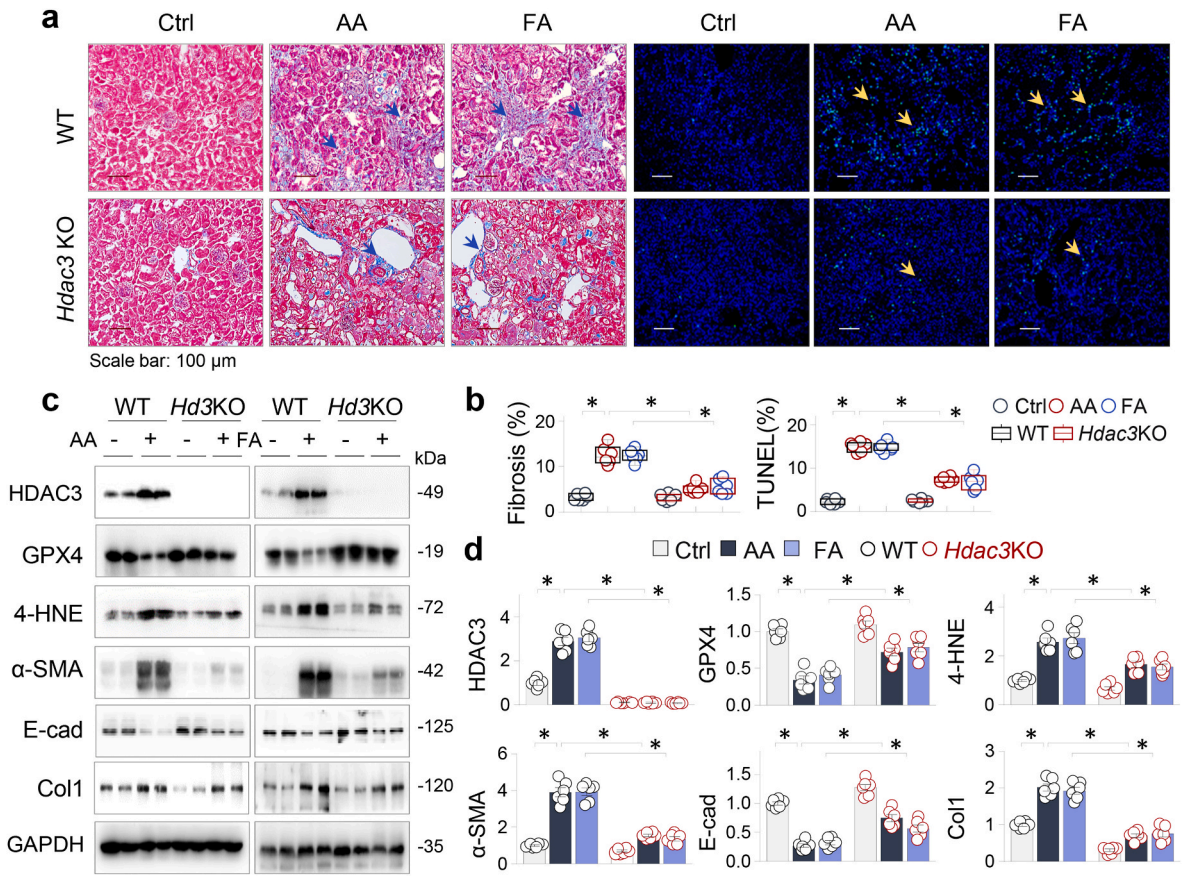

Fig. 3. HDAC3 knockout resists the GPX4 suppression, renal ferroptosis and fibrosis in AKI-CKD mice. (a) Representative photomicrographs of kidney sections of Masson's trichrome staining (the left half) and TUNEL staining (the right half) from wild-type (WT) and *Hdac3*KO mice treated with AA (5 mg/kg) or FA (250 mg/kg) for 14 days (n = 6). **(b)** Quantitation of renal fibrosis staining and TUNEL positive cells. The collagen deposition and TUNEL-positive cells were indicated by arrows. Data were presented as Box-and-whisker plots with data points, $^*P < 0.05$, two-way ANOVA. **(c)** Western blotting. The renal tissue homogenates were assayed for HDAC3, GPX4, 4-HNE, α-SMA, E-cad, Col1 and GAPDH. Two randomly-selected samples from each group were shown. **(d)** Quantification of Fig. 3c. Data were presented as means ± SEM; $^*P < 0.05$, two-way ANOVA.

b) comparing to the wilt-type control mice. Western blotting confirmed that HDAC3 was effectively knocked-out and the adverse expressions of α-SMA, E-cadherin, type 1 collagen, GPX4 and 4-HNE were milder in *Hdac3*KO mouse kidneys after AA or FA treatment (Fig. 3c and d), suggesting that the aberrant HDAC3 elevation plays a causative role in the ferroptosis and AKI-CKD transition.

3.4. HDAC3 inhibition by RGFP966 mitigates the ferroptotic and fibrotic renal injuries in AKI-CKD mice

To confirm the ferroptosis-resistant and renal-protective effects of *Hdac3*KO, we took a pharmacological approach and treated AA mice with a HDAC3-selective inhibitor RGFP966 that reportedly inhibited HDAC3 with an IC_{50} value of 80 nM while had no effective inhibition on other HDACs up to 15 μM [48]. The results showed that RGFP966 treatment did not change the normal renomorphology, but effectively reduced the AA-induced renal fibrosis (7.60 ± 0.63 % of RGFP966/AA vs. 14.29 ± 1.00 % of AA mice, $^*P < 0.05$, Fig. 4a and b), TUNEL-positive cell numbers (6.47 ± 0.69 % of RGFP966/AA vs. 16.09 ± 1.22 % of AA mice, $^*P < 0.05$, Fig. 4a and b) and induction of MDA (malondialdehyde), a marker of lipid peroxidation. Intriguingly, liproxstatin-1 (Lip-1), a spiroquinoxalinamine derivative inhibiting lipid peroxidation and ferroptosis without interfering with other forms of cell death [13], similarly reduced the renal fibrosis (9.53 ± 0.74 % of Lip-1/AA vs. 14.29 ± 1.00 % of AA mice, $^*P < 0.05$), TUNEL-positive cell numbers (11.76 ± 1.04 % of Lip-1/AA vs. 16.09 ± 1.22 % of AA mice, $^*P < 0.05$) and contents of MDA, although at less efficiency. In addition, we verified the ferroptotic alterations by electron microscopy examination and confirmed that AA-induced ferroptotic mitochondrial alterations, such as smaller mitochondrials and reduced cristae, were significantly alleviated by RG or Lip-1 (Fig. 4a). Meanwhile, RGFP966 significantly corrected the level alterations of α-SMA, type 1 collagen, E-cadherin, GPX4 and 4-HNE in AA-treated mice and enhanced the histone 3 acetylation under both basal and AA-treated conditions, whereas Lip-1 also improved the alterations of α-SMA, type 1 collagen, E-cadherin, and 4-HNE in AA-treated mice, although not significantly affected the levels of GPX4 or the acetylated histone 3 (Fig. 4c and d). Further, we assessed the renal tissue HDAC activities and found that AA treatment led to increased HDAC activities, which was significantly inhibited by RGFP966, but not by Lip-1 (Fig. 4e, the upper graph), supporting that the GPX4 suppression is mainly caused by HDAC3 enzymatic activities. We also assayed the renal functions by measuring serum creatinine (Cre) and blood urine nitrogen (BUN). Similarly, the AA increases of Cre and BUN were mitigated by RGFP966 and Lip-1 (Fig. 4e, the middle and low graphs). Together, these results indicate that GPX4 preservation by HDAC3 inhibition inhibits renal ferroptosis that contributes significantly to the renal fibrosis and functional loss of AKI-CKD mice.

3.5. HDAC3 inhibits GPX4 transcription in renal tubular epithelial cells

To directly test the causal relationship between the HDAC3 elevation and the GPX4 suppression, we measured the time course (0, 6, 12 and 24 h) expression alterations of HDAC3, GPX4, 4-HNE, and E-cadherin

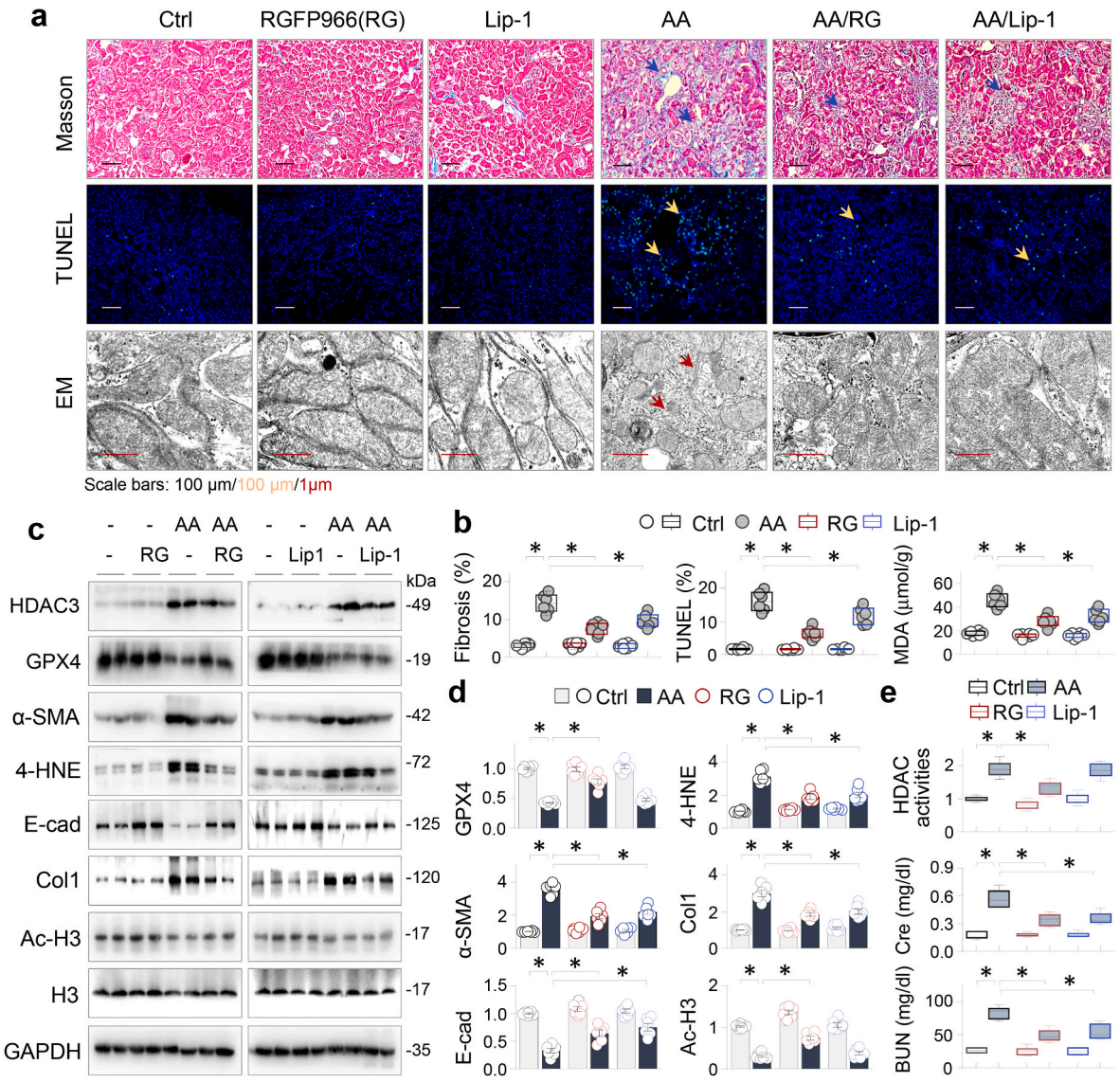

Fig. 4. HDAC3 inhibition by RGFP966 mitigates the ferroptotic and fibrotic renal injuries of AKI-CKD mice. The vehicle control (Ctrl) or AA (5 mg/kg)-treated mice were treated with or without RGFP966 (10 mg/kg) or liproxstatin-1 (Lip-1/L1, 10 mg/kg) for 3 days and 2 weeks (6 mice in each group). **(a)** Representative photomicrographs of kidney sections stained by Masson's trichrome (the upper half), TUNEL (the middle half) or EM (the lower half). The collagen deposition, TUNEL-positive cells and ferroptotic mitochondria were indicated by arrows. **(b)** Quantifications of renal fibrosis staining and TUNEL-positive cells in (a) and renal tissue MDA levels. Data were presented as Box-and-whisker plots with data points. **(c)** Western blotting. The renal tissue homogenates were assayed for HDAC3, GPX4, 4-HNE, α-SMA, E-cad, Col1, acetylated-histone 3 (Ac-H3), HDAC3 and GAPDH. Two samples from each group were shown. **(d)** Quantifications of (c). Data were presented as means ± SEM. **(e)** Renal tissue HDAC activity, serum creatinine (Cre) and blood urine nitrogen (BUN) were examined from the experimental mice indicated above. Data were presented as Box-and-whisker plots. $^*P < 0.05$, n = 6, two-way ANOVA.

after AA treatment in renal tubular HK2 cells. The results showed that HDAC3 started to increase at 6 h with concomitant reduction of GPX4 and E-cadherin, and 4-HNE induction (Fig. 5a); however RGFP966 effectively and similarly corrected the AA-induced protein expression alterations in both HK2 and primary renal tubular epithelial cells (PTC, Fig. 5b). Further, we treated the primary renal tubular epithelial cells from *Hdac3*KO and the control mice with or without AA and found that *Hdac3* knockout significantly resisted the AA-induced expression alterations of GPX4, 4-HNEand E-cadherin (Fig. 5c). Inversely, we overexpressed a flag-tagged HDAC3 in kidney HEK293 cells, which showed higher transfection efficiency. HDAC3 overexpression caused the similar expression alterations of GPX4, 4-HNE and E-cadherin incurred by AA (Fig. 5d). More importantly, when HDAC3 was overexpressed, the beneficial regulatory effects of RGFP966 on GPX4 and 4-HNE were significantly reduced (Fig. 5e). We also constructed a *Gpx4* promoter/luciferase reporter plasmid (*Gpx4*p-luc) and found that AA inhibited the promoter transcription, which was relieved by RGFP966 (Fig. 5f). These results indicate that HDAC3 acts upstream of GPX4 and inhibits *Gpx4* transcription. In addition, we performed C11-BODIPY straining and TUNEL assay of HK2 cells treated with AA or RSL3 (RAS-selective lethal 3), a GPX4 inhibitor that solely inactivates GPX4 protein leading to ferroptosis [49], in presence or absence of RGFP966. The results showed that the control cells displayed overwhelmingly the non-oxidized (N-) BODIPY (in red color, Fig. 5g, the upper part) and very few TUNEL positive cells (Fig. 5g, the lower panel) of resting cells, while both AA and RSL3 induced dramatic accumulations of oxidized (O-) BODIPY (in green color) and TUNEL positive cells. However, RGFP966 effectively reduced the oxidized BODIPY levels and TUNEL positive cell numbers induced by AA, but not that by RSL3 (Fig. 5g, the left and right panels). These data support that HDAC3 aberration transcriptionally inhibits GPX4, which causally affects lipid peroxidation and ferroptosis of renal tubular epithelial cells.

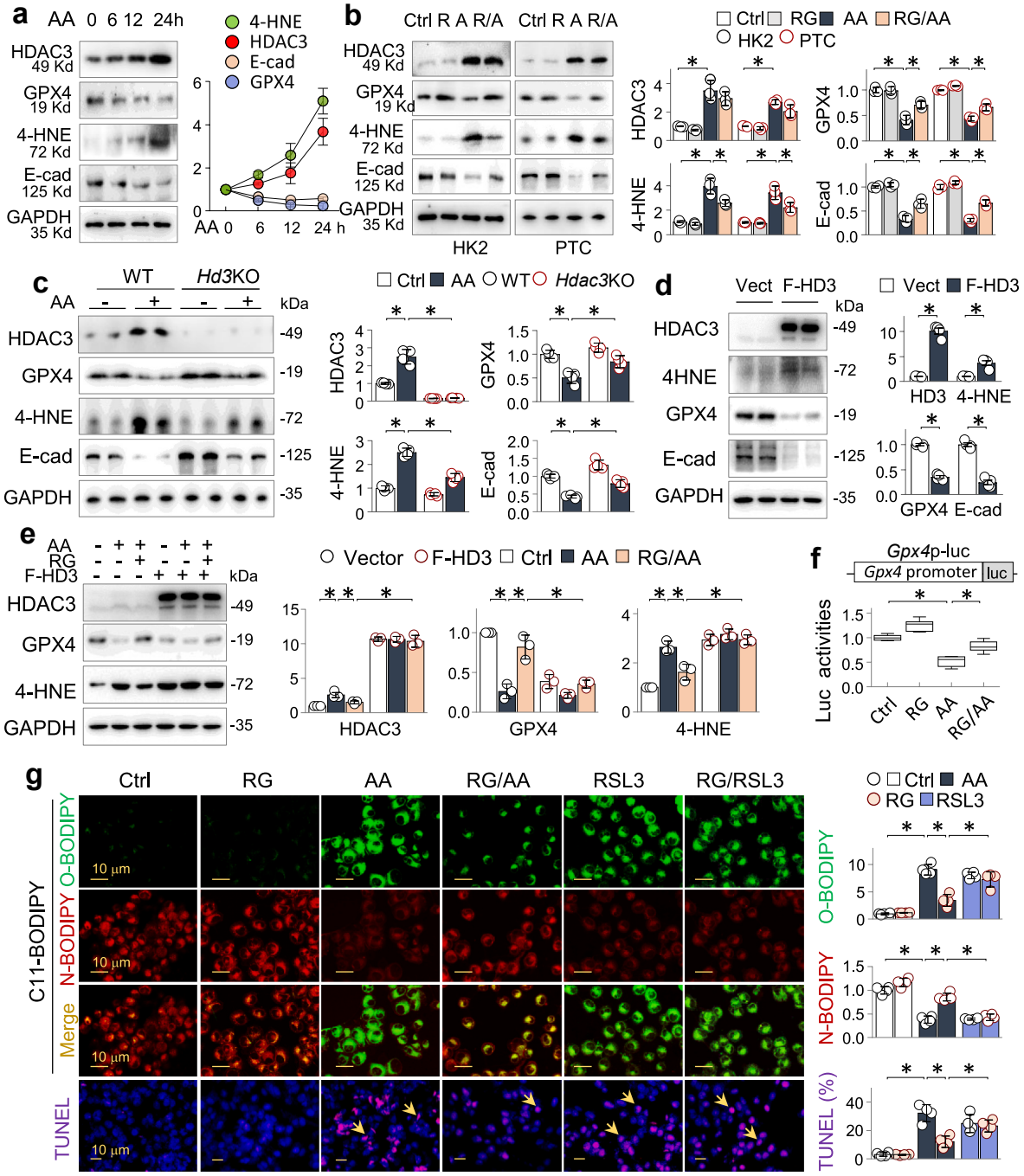

Fig. 5. HDAC3 inhibits GPX4 transcription in renal tubular epithelial cells. (a) Western blotting. HK2 cells were treated with AA (10 μg/ml) for 0 h, 6 h,12 h, 24 h and then assayed for HDAC3, GPX4, 4-HNE, and E-cadherin (E-cad). The quantitation was on the right side. **(b)** HK2 (the left panel) and the primary tubular epithelial cells (PTC, the right panel) were treated with AA (10 μg/ml) in presence or absence of RGFP966 (R,10 μM) for 24 h, and then cell lysates were assayed for HDAC3, GPX4, 4-HNE, and E-cadherin (E-cad). Quantifications were on the right side. **(c)** Western blotting. Primary renal tubule epithelial cell (PTC) from *Hdac3*WT and *Hdac3*KO mice (pretreated with tamoxifen as indicated in methods) were treated with or without AA (10 μg/ml) for 24 h, and then the cell lysates were tested for HDAC3, GPX4, 4-HNE, and E-cadherin (E-cad). **(d)** HEK293 cells were transfected with control plasmid (Vect) or a plasmid overexpressing flag-tagged HDAC3 (F-HD3). Twenty-four hours later, the cell lysates were assayed for HDAC3, GPX4, 4-HNE and E-cadherin (E-cad). **(e)** Western blotting. HEK293 cells transfected with the vector or F-HD3 plasmids were treated with AA (10 μg/ml) and/or RGFP966 (RG, 10 μM) for 24 h, and then the cell lysates were assayed for HDAC3, GPX4 and 4-HNE. The quantifications were on the right side. **(f)** Luciferase assay. HEK293 cells were transfected with a *Gpx4* promoter reporter *Gpx4*p-luc plus a renilla luciferase reporter, and then treated with AA (10 μg/ml) with or without RGFP966 (RG, 10 μM) for 24 h. Cell lysates were assayed for luciferase activities. The relative luciferase activities of fold changes were presented as Box-and-whisker plots of four repeated assays. *$P < 0.05$, two-way ANOVA. **(g)** Representative photomicrographs of C11-BODIPY and TUNEL staining. HK2 cells treated with RGFP966 (RG, 10 μM) in presence or absence of AA (10 μg/ml) or RSL3 (1 μM) for 24 h were stained by C11-BODIPY and TUNEL. Non-oxidized (N-) and oxidized (O-) BODIPY were in red and green respectively, and then merged. The positively-stained cells by TUNEL (TUNEL BrightRed kit) were indicated by arrows. The Quantifications of C11-BODIPY and TUNEL staining were on the right side. Data were presented as mean intensities/percentages of positive cell numbers ±SD of four repeated cell assays. *$P < 0.05$, one-way (a) or two-way ANOVA (the rest). (For interpretation of the references to color in this figure legend, the reader is referred to the Web version of this article.)

3.6. HDAC3 inhibition of Gpx4 transcription involves KLF5 (Kruppel-like factor 5)

HDAC3 lacks gene specificity and acts exclusively by forming a transcriptional repression complex with other transcriptional regulatory factors [27,50]. In order to understand how HDAC3 inhibits GPX4 transcription, we analyzed the *Gpx4* promoter by JASPAR (https://jaspar.genereg.net/) and found a number of binding motifs for various general transcriptional factors, such as Sp1(−43/gccccgcccaa, binding score 11.9437), C/EBPβ (−487/cttttgccat, 4.0259) and NF–1C (−6/-ttggct, 8.5204); however, a KLF5 (Kruppel-like factor 5) binding motif is close to the transcription starting site with very high binding score (−43/gccccgccca, 14.954). KLF5 is a renal epithelium-active and critical transcriptional factor that modulates both acute and chronic kidney injuries [51,52]. We found that KLF5 expression was upregulated in both AA and FA-treated kidneys (Fig. 6a). HK2 cells treated with a KLF5-selective inhibitor ML264 not only alleviated the AA-induced abnormal expressions of GPX4 and 4-HNE, but also reduced the HDAC3 induction (Fig. 6b and c). In addition, co-immunoprecipitation assay showed that renal HDAC3 was associated with KLF5 upon AA treatment (Fig. 6d), and together with a known HDAC3 co-repressor NCoR [28,50] inducibly bound to the KLF5 motif region of *Gpx4* promoter with correlated local histone 3 hypoacetylation, whereas RGFP966 inhibited the bindings and increased the local histone acetylation levels (Fig. 6e and f), which might involve several renal HDAC3-sensitive sites including histone 3 lysine 4 (H3K4), H3K9 and H4K5, as we demonstrated previously in mouse kidneys of UUO (unilateral ureter obstruction) [25]. These data suggest that HDAC3, KLF5 and NCoR jointly inhibit *Gpx4* transcription. To further prove the KLF5 involvement, we transfected the *Gpx4* promoter reporter plasmid *Gpx4*p-luc and treated the cells with AA in presence or absence of ML264 and RGFP966. The results showed that ML264 reduced the *Gpx4* promoter transcriptional suppression incurred by AA, which was further relieved by RGFP966 (Fig. 6g). Taken together, these results strongly support that HDAC3 converges with KLF5 to inhibit *Gpx4* transcription.

3.7. GPX4 restoration is critical for the anti-ferroptotic and renal protective effects of RGFP966

RGFP966 might affect the expression of a large number of HDAC3-modified genes. To determine the critical role of GPX4 restoration by RGFP966 in renal ferroptosis and AKI-CKD transition, we compared the anti-ferroptosis and anti-fibrosis effects of RGFP966 between control mice and mice receiving the GPX4 inhibitor RSL3, which induces GPX4 inhibition-mediated ferroptosis in both cell assay and in vivo animal studies [35,36]. The mice were further divided into control, RGFP966, AA, or RGFP966 plus AA groups. After RSL3 pretreatment, the renal GPX4 protein was substantially reduced (Fig. 7c and d, the top panel) and the RSL3-treated mice showed more renal fibrotic alterations under basal (5.178 ± 0.6 % of RSL3 vs. 3.11 ± 0.21 % of Ctrl) and AA-treated condition (21.01 ± 0.91 % of RSL3/AA vs. 16.63 ± 0.89 % of Ctrl/AA, $^*P < 0.05$, Fig. 7a, the upper panel, and b), more TUNEL-positive cells (5.19 ± 0.6 % of RSL3 vs. 1.78 ± 0.21 % of control; 23.24 ± 1.12 % of RSL3/AA vs. 16.03 ± 1.12 % of Ctrl/AA, Fig. 7a, the lower panel, and b) and higher contents of MDA (malondialdehyde), a marker of lipid peroxidation [53] (Fig. 7b). As anticipated, RGFP966 treatment

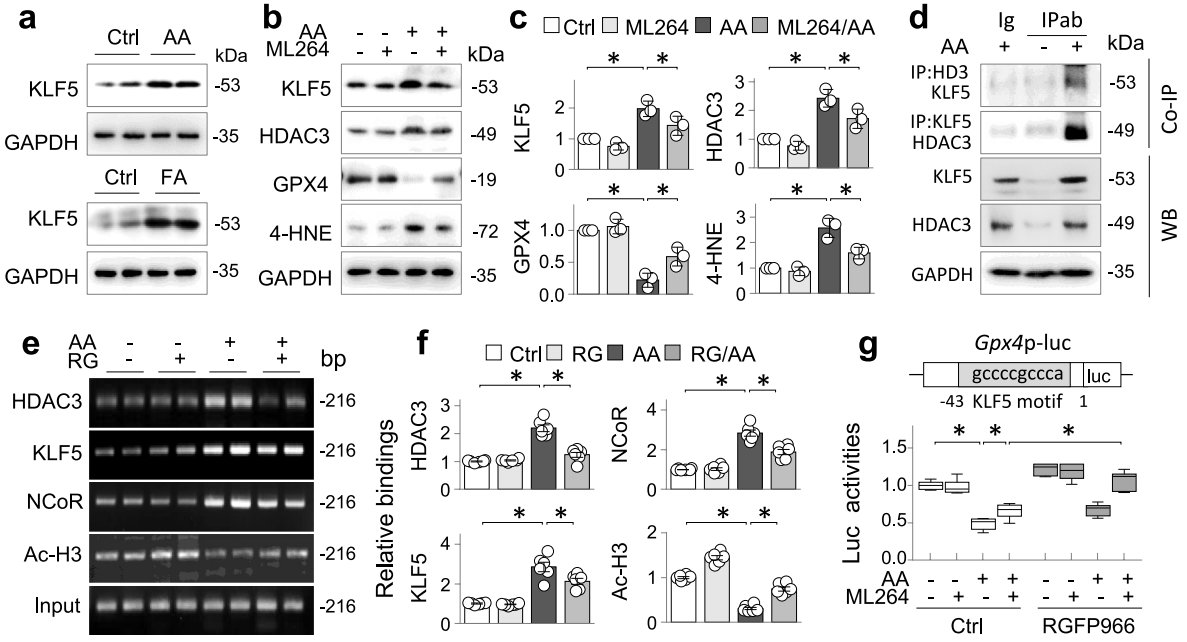

Fig. 6. HDAC3 inhibition of *Gpx4* transcription involves KLF5. (a) Western blotting. Renal tissue homogenates from control (Ctrl) and AA (5 mg/kg, 3 days)/FA (250 mg/kg, 3 days)-treated mice were assayed for KLF5 with GAPDH served as loading control. Two samples from each group were shown. **(b)** Western blotting. HK2 cells were treated with AA (10 μg/ml) with or without ML264 (10 μM) for 24 h, and then cell lysates were assayed for GPX4, 4-HNE, KLF5, E-cadherin (E-cad) and HDAC3. **(c)** Quantifications of (b). Data were presented as means ± SD of three repeated assays, $^*P < 0.05$, two-way ANOVA. **(d)** Co-IP assay. Renal tissue homogenates of control and the AA mice (5 mg/kg, 3 days) were immunoprecipitated with isoform-matched immunoglobulin (Ig) or antibody (IPab) to HDAC3 (HD3) or KLF5, and then immunoprecipitants were assessed for HDAC3 or KLF5 by western blotting reciprocally (the upper panel). The non-IP lysates were assayed for HDAC3 and KLF5 as input controls (the lower panel). **(e)** ChIP assay. The renal tissues from AA-treated mice (5 mg/kg, 3 days) were immunoprecipitated with antibodies to HDAC3, KLF5, NCoR, or acetylated histone 3 (Ac-H3), respectively, and then the genomic DNA (Input) and the antibody-bound DNAs were PCR-amplified with primers covering the KLF5 motif on *Gpx4* promoter. The PCR products were analyzed on 1.5 % agarose gels. Two representative samples from each group were shown. **(f)** Quantification of (e). Data were presented as relative mean binding intensities ±SEM of all 6 samples, $^*P < 0.05$, two-way ANOVA. **(g)** Luciferase assay. HEK293 cells were transfected with *Gpx4* promoter reporter (*Gpx4*p-luc) plus a renilla luciferase reporter control, and then treated with AA (10 μg/ml) with or without ML264 (KLF5 inhibitor, 10 μM) in absence or presence of RGFP966 (10 μM) for 24 h. The luciferase activities of *Gpx4*p-luc were normalized with the renilla's, and the relative fold changes of *Gpx4*p-luc luciferase activities were presented as Box-and-whisker plots of four repeated assays, $^*P < 0.05$, three-way ANOVA followed by Tukey's post-hoc test.

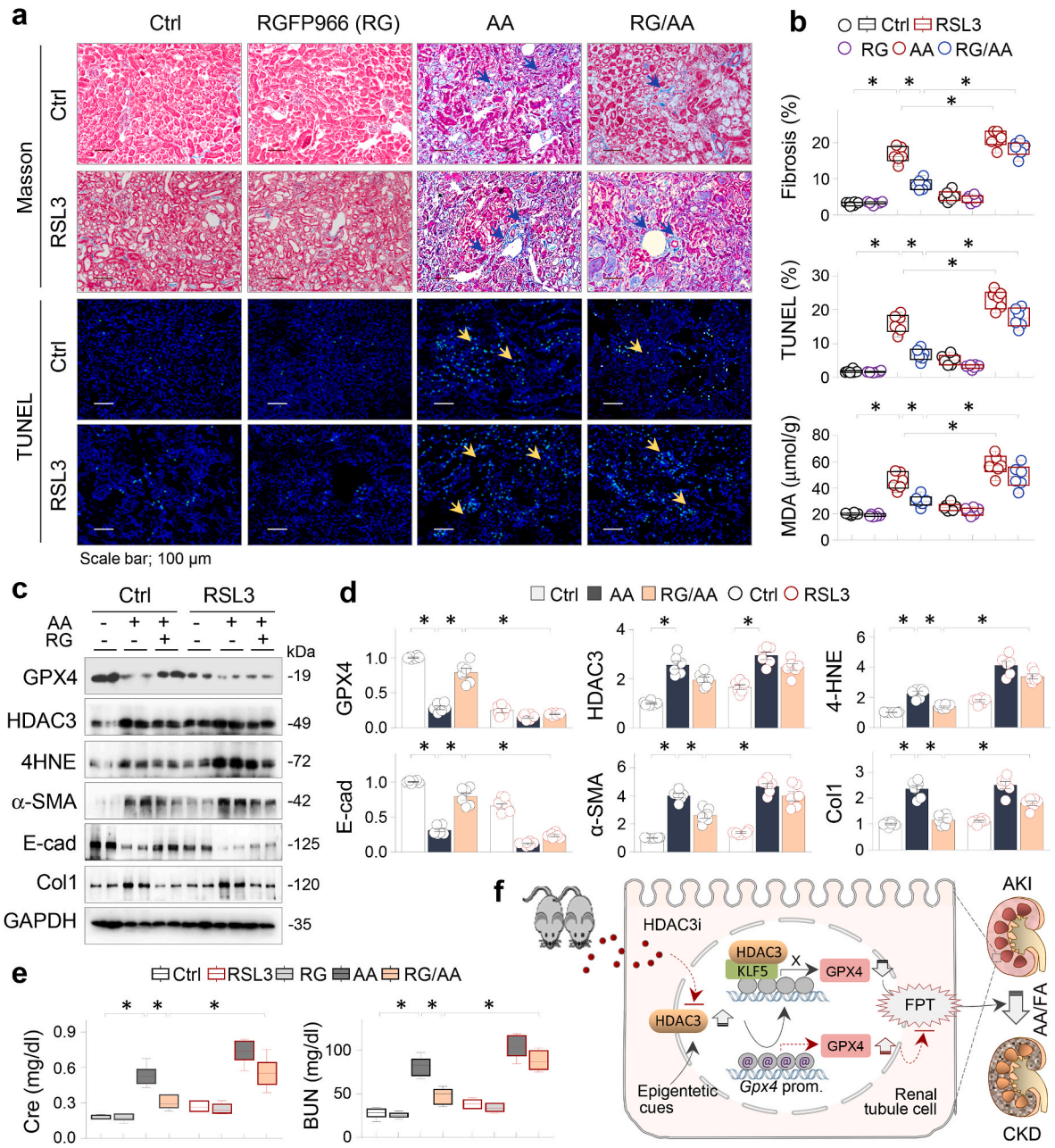

Fig. 7. GPX4 restoration is critical for the anti-ferroptotic and renal protective effects of RGFP966. Mice receiving Control vehicle (Ctrl) or RSL3 (5 mg/kg) were grouped into Control (Ctrl), RGFP966 (RG), AA, and RG-treated AA mice (n = 6, 14 days). **(a)** Representative microphotographs of kidney sections stained by Masson's trichrome (the upper panel) or TUNEL (the lower panel). The collagen deposition and TUNEL-positive cells were indicated by arrows. **(b)** Quantitation of fibrosis staining and TUNEL-positive cells in Fig.7a and renal tissue MDA levels. Data were presented as Box-and-whisker plots with data points. **(c)** Western blotting. The renal tissues from the experimental mice in (a) were assayed for HDAC3, GPX4, 4-HNE, α-SMA, E-cadherin (E-cad), collagen 1 (Col1), and GAPDH. Two randomly-selected samples from each group were shown. **(d)** Quantification of (c). Data in **(b)** and **(d)** were presented as means ± SEM. **(e)** Serum levels of creatinine (Cre) and blood urea nitrogen (BUN). Data were presented as Box-and-whisker plots. *$P < 0.05$, three-way ANOVA followed by Tukey's post-hoc test. **(f)** A schematic diagram of sequential HDAC3 elevation and binding together with KLF5 to *Gpx4* promoter, resulting in *Gpx4* promoter hypoacetylated (@) and transcriptional suppression, increased lipid peroxidation (LP) and ferroptosis (FPT), which promoted AKI-CKD transition induced by AA and FA (solid lines). On the other hand, HDAC3-selective inhibition by RGFP966 (HDAC3i) effectively reduced the *Gpx4* suppression and renal ferroptosis, and prevented the AKI-CKD transition (dashed lines).

significantly reduced the renal fibrosis (16.63 ± 0.89 % of AA vs. 8.43 ± 0.62 % of RGFP966/AA, *$P < 0.05$), TUNEL-positive cell numbers (16.03 ± 1.12 % of AA vs. 6.72 ± 0.73 % of RGFP/AA, *$P < 0.05$) and MDA contents in the control mice, but RSL3 treatment largely abrogated the beneficial regulatory effects (Fig. 7a and b). Similarly, the AA-induced abnormal expressions of GPX4, HDAC3, α-SMA, E-cadherin, type 1 collagen, 4-HNE were effectively corrected by RGFP966 in the control mice, but the effects were significantly reduced in mice treated with RSL3 (Fig. 7c and d). Also, the serum creatinine and BUN showed similar alteration patterns (Fig. 7e). These results strongly indicate that GPX4 restoration by RGFP966 is essential for its anti-ferroptosis and renoprotective functions during AKI-CKD progression.

4. Discussion

In this study, we have investigated the potential roles of HDAC3-

incurred epigenetic GPX4 suppression and renal ferroptosis in AKI-CKD progression. We found that the AKI-CKD kidneys induced by AA and FA displayed early GPX4 suppression due to aberrant HDAC3 elevation, leading to increased lipid peroxidation and renal ferroptosis (FPT) that promote AKI-CKD transition. On the other hand, administration of a HDAC3-selective inhibitor RGFP966 effectively preserved GPX4, reduced the renal ferroptotic/fibrotic damage and prevented the AKI-CKD transition (Fig. 7f). Thus, our study identified an important epigenetic pathway of renal ferroptosis during AKI-CKD progression with potential prophylactic or therapeutic implications.

AKI-CKD transition is associated with various forms of regulated cell death of tubular epithelial cells and other cell types, such as endothelia and podocytes, which presumably interplay in a positive fashion that promotes renal tubule injury, myofibroblast transdifferentiation and fibrogenesis [54]. Previous study suggests that ferroptosis, but not necroptosis, is the primary cause of AKI [55], pinpointing a key pathological event that influences AKI-CKD transition. Our study focused on tubular epithelial cells and demonstrated that HDAC3 inhibition preserved GPX4 and GPX4-dependently reduced the tubular epithelial ferroptosis, improved the renal fibrosis and renal functions, supporting that HDAC3 aberration-associated GPX4 suppression plays a critical role in renal tubular epithelial ferroptosis and AKI-CKD transition. It is noteworthy that our study does not exclude ferroptotic damage from other cell types that might contribute to the AKI-CKD transition. Future study with cell type-specific gene knockout approaches might clarify this issue.

Identification of aberrant HDAC3 elevation and its inhibition of *Gpx4* transcription critically involved to renal epithelial ferroptosis during AKI-CKD progression is an important discovery of our study. AKI-CKD transition is greatly affected by various epigenetic modifications, including DNA methylation and microRNA interferences [23,24]. GPX4 is mainly regulated at the enzymatic activity or protein stability levels [56]. For example, when GSH (glutathione) is depleted due to impaired cysteine/glutamate metabolisms, GPX4 is inactivated [56]. Many synthetic small compounds, such as RSL3, ML162 and FIN56, have been developed to induce ferroptotic cell death for cancer therapy via directly inactivating GPX4 [57]. Some natural products of terpenoids, flavonoids or polyphenols can positively or negatively affect ferroptosis via regulating GPX4 [14,57–59], however most these studies lack clarified pharmacological mode of actions. We found that the *Gpx4* suppression occurred substantially at transcription level with marked HDAC3 elevation in AKI-CKD mouse kidneys, whereas a HDAC3 selective inhibitor RGFP966 effectively corrected the GPX4 suppression, ferroptotic and fibrotic alterations and renal function in these mice. Since epigenetic modifications are mechanistically interconnected on a particular gene expression, our study not only reveals an important epigenetic feature of *Gpx4* suppression and renal ferroptosis, but also suggests that beneficial regulation of GPX4 and ferroptosis can be achieved by HDAC3 intervention and potentially by other epigenetic modulations.

One of the intriguing observations of our study is the KLF5 involvement in the HDAC3 inhibition of *Gpx4* transcription. KLF5 promoted renal fibrosis in UUO and 5/6 nephrectomy kidneys, and conversely, KLF5 haploinsufficiency partially protects against the renal epithelial injuries [60,61]. KLF5 can either positively or negatively regulate the target gene transcription. For example, KLF5 promotes the transcription of pro-fibrotic genes [61], but inhibits the transcription of pro-inflammatory cytokines under ischemic-reperfusion conditions [62] and switches between an activator or repressor of several genes involved in lipid oxidation, such as *Cpt1b, Ucp2 and Ucp3,* in a sumoylation modification-dependent manner [63]. We showed that HDAC3 and KLF5 inducibly associated and bound to the KLF5 motif area of *Gpx4* promoter after AA treatment with local histone 3 hypoacetylation (Fig. 6d and e) and *Gpx4* transcriptional suppression, which were relieved by pharmacological inhibition of HDAC3 or KLF5, respectively. On the other hand, HDAC3 promoter actually contains several putative KLF5 binding motifs (−56/-47, −30/-21 and 35/44, by JASPAR analysis), and KLF5 inhibition by ML264 decreased the HDAC3 induction (Fig. 6b and c). These data suggest that KLF5 is another important pro-ferroptotic regulator during AKI-CKD progression and acts, like many transcription factors, via at least a dual mode of transcriptional regulation. Namely, it upregulates HDAC3 and meanwhile assists HDAC3 inhibition of *Gpx4* transcription, which sensitizes renal epithelial cells to ferroptosis.

In conclusion, we have identified that *Gpx4* transcriptional suppression driven by HDAC3 aberration is an epigenetic feature of renal tubular epithelial ferroptosis that contributes significantly to AKI-CKD progression. Since epigenetic modifications and some regulated cell death events are reportedly reversible and epigenetic drugs are emerging as potent clinical options, our results provide strong evidence that strategies targeting *Gpx4* transcriptional repression by epigenetic HDAC3 intervention are promising to reduce renal ferroptosis and potentially prevent AKI-CKD progression and other ferroptotic kidney disorders.

Author contributions

LZ, investigation, data acquisition and analysis, manuscript drafting; FC, JD and RW, cell assay and animal study assistance; GB, DX, YZ, YD, WL and ZY, data analysis and resource support; WC, conception and experimental design, data interpretation and arrangement, manuscript writing and revising. All authors approved the final version of the manuscript.

Data availability

All data related to this paper are available from the corresponding author upon reasonable request.

Declaration of competing interest

The authors declare that there are no conflicts of interest.

Acknowledgements

This study was supported by research grants 82300780 (FC), 82000704 (WL) and 81970577 (WC) from National Nature & Science Foundation of China (NFSC).

Appendix A. Supplementary data

Supplementary data to this article can be found online at https://doi.org/10.1016/j.redox.2023.102939.

References

[1] I.D. Bucaloiu, et al., Increased risk of death and de novo chronic kidney disease following reversible acute kidney injury, Kidney Int. 81 (5) (2012) 477–485.
[2] F. Tanemoto, I. Mimura, Therapies targeting epigenetic alterations in acute kidney injury-to-chronic kidney disease transition, Pharmaceuticals 15 (2) (2022) 123.
[3] M. Mercado, D. Smith, E. Guard, Acute kidney injury: diagnosis and management, Am. Fam. Physician 100 (11) (2019) 687–694.
[4] H.M. Tang, H.L. Tang, Cell recovery by reversal of ferroptosis, Biol. Open 8 (6) (2019) bio043182.
[5] H.M. Tang, H.L. Tang, Anastasis: recovery from the brink of cell death, R. Soc. Open Sci. 5 (2018), 180442.
[6] X. Chen, et al., Requirement for the histone deacetylase Hdac3 for the inflammatory gene expression program in macrophages, Proc. Natl. Acad. Sci. USA 109 (42) (2012) E2865–E2874.
[7] D. Bertheloot, E. Latz, B.S. Franklin, Necroptosis, pyroptosis and apoptosis: an intricate game of cell death, Cell. Mol. Immunol. 18 (5) (2021) 1106–1121.
[8] X. Jiang, B.R. Stockwell, M. Conrad, Ferroptosis: mechanisms, biology and role in disease, Nat. Rev. Mol. Cell Biol. 22 (4) (2021) 266–282.
[9] D. Tang, et al., Ferroptosis: molecular mechanisms and health implications, Cell Res. 31 (2) (2020) 107–125.
[10] G. Wu, et al., Glutathione metabolism and its implications for health, J. Nutr. 134 (3) (2004) 489–492.

[11] B.R. Stockwell, et al., Ferroptosis: a regulated cell death nexus linking metabolism, redox biology, and disease, Cell 171 (2) (2017) 273–285.
[12] Y. Qiu, et al., The application of ferroptosis in diseases, Pharmacol. Res. 159 (2020), 104919.
[13] J.P. Friedmann Angeli, et al., Inactivation of the ferroptosis regulator Gpx4 triggers acute renal failure in mice, Nat. Cell Biol. 16 (12) (2014) 1180–1191.
[14] Y. Wang, et al., Quercetin alleviates acute kidney injury by inhibiting ferroptosis, J. Adv. Res. 28 (2021) 231–243.
[15] D. Li, et al., Nuciferine protects against folic acid-induced acute kidney injury by inhibiting ferroptosis, Br. J. Pharmacol. 178 (5) (2021) 1182–1199.
[16] M. Guerrero-Hue, et al., Curcumin reduces renal damage associated with rhabdomyolysis by decreasing ferroptosis-mediated cell death, Faseb. J. 33 (8) (2019) 8961–8975.
[17] D. Martin-Sanchez, et al., Ferroptosis and kidney disease, Nefrologia 40 (4) (2020) 384–394.
[18] Y. Pei, et al., Epigenetic regulation of ferroptosis-associated genes and its implication in cancer therapy, Front. Oncol. 12 (2022), 771870.
[19] O. Rroji, et al., Epigenetic regulators of neuronal ferroptosis identify novel therapeutics for neurological diseases: HDACs, transglutaminases, and HIF prolyl hydroxylases, Neurobiol. Dis. 147 (2021), 105145.
[20] M. Zille, et al., Ferroptosis in neurons and cancer cells is similar but differentially regulated by histone deacetylase inhibitors, ENEURO 6 (1) (2019), pp. 0263–18.
[21] I.V. Gregoretti, Y.M. Lee, H.V. Goodson, Molecular evolution of the histone deacetylase family: functional implications of phylogenetic analysis, J. Mol. Biol. 338 (1) (2004) 17–31.
[22] S. Balasubramanian, E. Verner, J. Buggy, Isoform-specific histone deacetylase inhibitors: the next step? Cancer Lett. 280 (2) (2009) 211–221.
[23] Z. Li, N. Li, Epigenetic modification drives acute kidney injury-to-chronic kidney disease progression, Nephron 145 (6) (2021) 737–747.
[24] R. Rodríguez-Romo, et al., Epigenetic regulation in the acute kidney injury to chronic kidney disease transition, Nephrology 20 (10) (2015) 736–743.
[25] F. Chen, et al., Histone deacetylase 3 aberration inhibits Klotho transcription and promotes renal fibrosis, Cell Death Differ. 28 (3) (2021) 1001–1012.
[26] W. Lin, et al., Klotho restoration via acetylation of Peroxisome Proliferation–Activated Receptor γ reduces the progression of chronic kidney disease, Kidney Int. 92 (3) (2017) 669–679.
[27] Y.D. Wen, et al., The histone deacetylase-3 complex contains nuclear receptor corepressors, Proc. Natl. Acad. Sci. U. S. A. 97 (13) (2000) 7202–7207.
[28] J. Li, et al., Both corepressor proteins SMRT and N-CoR exist in large protein complexes containing HDAC3, EMBO J. 19 (16) (2000) 4342–4350.
[29] P. Joshi, et al., The functional interactome landscape of the human histone deacetylase family, Mol. Syst. Biol. 9 (1) (2013) 672.
[30] Y. Shi, et al., RIPK3 blockade attenuates kidney fibrosis in a folic acid model of renal injury, Faseb. J. 34 (8) (2020) 10286–10298.
[31] M.M. Perales-Quintana, et al., Metabolomic and biochemical characterization of a new model of the transition of acute kidney injury to chronic kidney disease induced by folic acid, PeerJ 7 (2019) e7113.
[32] T. Baudoux, et al., Experimental aristolochic acid nephropathy: a relevant model to study AKI-to-CKD transition, Front. Med. 9 (2022).
[33] Q. Kuang, et al., Selective Wnt/β-Catenin pathway activation concomitant with sustained overexpression of miR-21 is responsible for aristolochic acid-induced AKI-to-CKD transition, Front. Pharmacol. 12 (2021).
[34] B. Zhang, et al., Liproxstatin-1 attenuates unilateral ureteral obstruction-induced renal fibrosis by inhibiting renal tubular epithelial cells ferroptosis, Cell Death Dis. 12 (9) (2021) 843.
[35] F. Deng, et al., The gut microbiota metabolite capsiate promotes Gpx4 expression by activating TRPV1 to inhibit intestinal ischemia reperfusion-induced ferroptosis, Gut Microb. 13 (1) (2021).
[36] Y. Cui, et al., Microglia and macrophage exhibit attenuated inflammatory response and ferroptosis resistance after RSL3 stimulation via increasing Nrf2 expression, J. Neuroinflammation 18 (1) (2021).
[37] D. Li, et al., Nuciferine protects against folic acid-induced acute kidney injury by inhibiting ferroptosis, Br. J. Pharmacol. 178 (5) (2021) 1182–1199.
[38] E. Charafe-Jauffret, et al., Immunophenotypic analysis of inflammatory breast cancers: identification of an'inflammatory signature', J. Pathol. 202 (3) (2004) 265–273.
[39] E.R. Smith, et al., TGF-beta1 Modifies Histone Acetylation and Acetyl-Coenzyme A Metabolism in Renal Myofibroblasts, Am J Physiol Renal Physiol, 2019.
[40] A. Bernhardt, et al., Inflammatory cell infiltration and resolution of kidney inflammation is orchestrated by the cold-shock protein Y-box binding protein-1, Kidney Int. 92 (5) (2017) 1157–1177.
[41] C. Luo, et al., Wnt9a promotes renal fibrosis by accelerating cellular senescence in tubular epithelial cells, J. Am. Soc. Nephrol. 29 (4) (2018) 1238–1256.
[42] E.H.W. Pap, et al., Ratio-fluorescence microscopy of lipid oxidation in living cells using C11-BODIPY581/591, FEBS (Fed. Eur. Biochem. Soc.) Lett. 453 (3) (1999) 278–282.
[43] L. Liu, et al., TGF-β induces miR-30d down-regulation and podocyte injury through Smad2/3 and HDAC3-associated transcriptional repression, J. Mol. Med. 94 (3) (2015) 291–300.
[44] Q. Gao, et al., Inhibition of DNA methyltransferase aberrations reinstates antioxidant aging suppressors and ameliorates renal aging, Aging Cell 21 (1) (2021), e13526.
[45] M. Lu, et al., GSK3beta-mediated Keap1-independent regulation of Nrf2 antioxidant response: a molecular rheostat of acute kidney injury to chronic kidney disease transition, Redox Biol. 26 (2019), 101275.
[46] T. Baudoux, et al., Experimental aristolochic acid nephropathy: a relevant model to study AKI-to-CKD transition, Front. Med. 9 (2022), 822870.
[47] L.J. Yan, Folic acid-induced animal model of kidney disease, Anim. Models Exp. Med. 4 (4) (2021) 329–342.
[48] M. Malvaez, et al., HDAC3-selective inhibitor enhances extinction of cocaine-seeking behavior in a persistent manner, Proc. Natl. Acad. Sci. USA 110 (7) (2013) 2647–2652.
[49] W.S. Yang, B.R. Stockwell, Synthetic lethal screening identifies compounds activating iron-dependent, nonapoptotic cell death in oncogenic-RAS-harboring cancer cells, Chem. Biol. 15 (3) (2008) 234–245.
[50] P. Karagianni, J. Wong, HDAC3: taking the SMRT-N-CoRrect road to repression, Oncogene 26 (37) (2007) 5439–5449.
[51] J. Li, et al., Roles of Krüppel-like factor 5 in kidney disease, J. Cell Mol. Med. 25 (5) (2021) 2342–2355.
[52] M.J. Rane, Y. Zhao, L. Cai, Krüppel-like factors (KLFs) in renal physiology and disease, EBioMedicine 40 (2019) 743–750.
[53] P. Liu, et al., Ferrostatin-1 alleviates lipopolysaccharide-induced acute lung injury via inhibiting ferroptosis, Cell. Mol. Biol. Lett. 25 (2020) 10.
[54] J.T. Kurzhagen, et al., AKI: an increasingly recognized risk factor for CKD development and progression, J. Nephrol. 33 (6) (2020) 1171–1187.
[55] D. Martin-Sanchez, et al., Ferroptosis, but not necroptosis, is important in nephrotoxic folic acid–induced AKI, J. Am. Soc. Nephrol. 28 (1) (2017) 218–229.
[56] X. Chen, et al., Characteristics and biomarkers of ferroptosis, Front. Cell Dev. Biol. 9 (2021), 637162.
[57] C. Ge, et al., Emerging mechanisms and disease implications of ferroptosis: potential applications of natural products, Front. Cell Dev. Biol. 9 (2022), 774957.
[58] W. Guo, et al., Epigenetic studies of Chinese herbal medicine: pleiotropic role of DNA methylation, Front. Pharmacol. 12 (2021), 790321.
[59] Z. Huang, et al., Epigenetic regulation of active Chinese herbal components for cancer prevention and treatment: a follow-up review, Pharmacol. Res. 114 (2016) 1–12.
[60] K. Fujiu, I. Manabe, R. Nagai, Renal collecting duct epithelial cells regulate inflammation in tubulointerstitial damage in mice, J. Clin. Invest. 121 (9) (2011) 3425–3441.
[61] Z. Li, et al., The profibrotic effects of MK-8617 on tubulointerstitial fibrosis mediated by the KLF5 regulating pathway, Faseb. J. 33 (11) (2019) 12630–12643.
[62] Y. Li, et al., KLF5 overexpression attenuates cardiomyocyte inflammation induced by oxygen-glucose deprivation/reperfusion through the PPARγ/PGC-1α/TNF-α signaling pathway, Biomed. Pharmacother. 84 (2016) 940–946.
[63] Y. Oishi, et al., SUMOylation of Krüppel-like transcription factor 5 acts as a molecular switch in transcriptional programs of lipid metabolism involving PPAR-δ, Nat. Med. 14 (6) (2008) 656–666.